



## Research article

# The efficacy of the anticancer 3-bromopyruvate is potentiated by antimycin and menadione by unbalancing mitochondrial ROS production and disposal in U118 glioblastoma cells



Maya Petricciuolo, Magdalena Davidescu, Katia Fettucciari, Leonardo Gatticchi, Stefano Brancorsini, Rita Roberti, Lanfranco Corazzi<sup>\*</sup>, Lara Macchioni<sup>\*\*</sup>

Department of Experimental Medicine, University of Perugia, 06132, Perugia, Italy

## ARTICLE INFO

## Keywords:

Glioblastoma cells  
3-Bromopyruvate  
Mitochondrial ROS  
Cytochrome c  
Antimycin A  
Menadione  
Biological sciences  
Biochemistry  
Oxidative stress  
Cancer research

## ABSTRACT

Metabolic reprogramming of tumour cells sustains cancer progression. Similar to other cancer cells, glioblastoma cells exhibit an increased glycolytic flow, which encourages the use of antiglycolytics as an effective complementary therapy. We used the antiglycolytic 3-bromopyruvate (3BP) as a metabolic modifier to treat U118 glioblastoma cells and investigated the toxic effects and the conditions to increase drug effectiveness at the lowest concentration. Cellular vitality was not affected by 3BP concentrations lower than 40  $\mu\text{M}$ , although p-Akt dephosphorylation, p53 degradation, and ATP reduction occurred already at 30  $\mu\text{M}$  3BP. ROS generated in mitochondria were enhanced at 30  $\mu\text{M}$  3BP, possibly by unbalancing their generation and their disposal because of glutathione peroxidase inhibition. ROS triggered JNK and ERK phosphorylation, and cyt c release outside mitochondria, not accompanied by caspases-9 and -3 activation, probably due to 3BP-dependent alkylation of cysteine residues at caspase-9 catalytic site. To explore the possibility of sensitizing cells to 3BP treatment, we exploited 3BP effects on mitochondria by using 30  $\mu\text{M}$  3BP in association with antimycin A or menadione concentrations that in themselves exhibit poor toxicity. 3BP effect on cyt c release and cell vitality loss was potentiated due the greater oxidative stress induced by antimycin or menadione association with 3BP, supporting a preeminent role of mitochondrial ROS in 3BP toxicity. Indeed, the scavenger of mitochondrial superoxide MitoTEMPO counteracted 3BP-induced cyt c release and weakened the potentiating effect of 3BP/antimycin association. In conclusion, the biochemical mechanisms leading U118 glioblastoma cells to viability loss following 3BP treatment rely on mitochondrial ROS-dependent pathways. Their potentiation at low 3BP concentrations is consistent with the goal to minimize the toxic effect of the drug towards non-cancer cells.

## 1. Introduction

Multiple genetic alterations are typical features of cancer cells, and multi-target agents are needed to meet the diverse requirements in cancer treatment. Auto-protection mechanisms against cytotoxic compounds are promoted in cancer cells, including overexpression of the ABC family transporters (Choudhuri and Klaassen, 2006), multidrug resistance proteins (Ni et al., 2011), and breast cancer resistance protein (Natarajan et al., 2012), as well as anti-apoptotic factors, responsible for insensitivity to drug-induced apoptosis, and drug-detoxifying enzymes (Gottesman, 2002). The “metabolic reprogramming” that sustains cancer cells includes increased glycolysis, aimed to provide the ATP levels

needed for cancer progression, which makes glycolytic inhibitors particularly effective drugs when mitochondrial defects are present or under hypoxic conditions.

Although enhanced glycolysis is the main metabolic feature of cancer cells and the target of antiglycolytics, other targets related to energy metabolism may be considered in the approaches oriented to remodel metabolic pathways, such as the modulation of mitochondrial activities aimed to contrast drug resistance. The antiglycolytic 3-bromopyruvate (3BP) is a reactive non-specific drug that can act as a metabolic modifier by interfering with glycolysis and oxidative phosphorylation in cancer cells (Shoshan, 2012; Lis et al., 2016; Ko et al., 2019; Azevedo-Silva et al., 2016; Fan et al., 2019). The mitochondrial hexokinase-II is

\* Corresponding author.

\*\* Corresponding author.

E-mail addresses: [lanfranco.corazzi@unipg.it](mailto:lanfranco.corazzi@unipg.it) (L. Corazzi), [lara.macchioni@unipg.it](mailto:lara.macchioni@unipg.it) (L. Macchioni).

<https://doi.org/10.1016/j.heliyon.2020.e05741>

Received 25 August 2020; Received in revised form 6 November 2020; Accepted 11 December 2020

2405-8440/© 2020 The Authors. Published by Elsevier Ltd. This is an open access article under the CC BY-NC-ND license (<http://creativecommons.org/licenses/by-nc-nd/4.0/>).

the main target since its activity is specifically blocked by the formation of a pyruvyl adduct after reacting with 3BP at the surface of the outer mitochondrial membrane (Mathupala et al., 2009; Galina, 2014). 3BP is suitable for overcoming cancer resistance in conventional chemotherapy. Cancer stem cells or tumour-initiating cells in epithelial ovarian carcinoma exhibit high chemoresistance, which correlates with upregulation of hexokinase-II and voltage-dependent anion channel (VDAC), known to form a survival-promoting mitochondrial complex. Indeed, repeated cisplatin treatment can lead to a multiresistant tumour cell population with stem cell features. 3BP contrasts the resistance developed by the drug by dissociating the hexokinase-II/VDAC complex (Wintzell et al., 2012). In malignant tumour cell lines, 3BP inhibits ATPase activity, reduces ATP levels, and reverses chemoresistance by antagonizing drug efflux by acting on the ATP-binding cassette transporters (Nakano et al., 2011; Wu et al., 2014). Furthermore, 3BP increases the production of reactive oxygen species (ROS) (Ihrlund et al., 2008; Kim et al., 2008; Macchioni et al., 2011a), induces ER stress, and inhibits translation (Ganapathy-Kanniappan et al., 2010), possibly contributing to cell death.

Low levels of ROS regulate cellular signalling and play an important role in cell proliferation under non-stress conditions (Burdon, 1995). However, when cells are exposed to various stress agents, including anticancer drugs, ROS increase to promote apoptosis by stimulating pro-apoptotic signalling molecules, such as ASK, JNK, and p38. Unfortunately, prolonged treatment with the drug reduces ROS levels and confers resistance by inducing regulatory genes that act on antioxidant systems. Indeed, in cancer cells drug resistance is characterized by higher expression of catalase (Bechtel and Bauer, 2009). In general, evidence indicating that reduced ROS levels could be one way permitting cancer cells to acquire drug resistance is accumulating (Maiti, 2012).

Similar to other cancer cells, an increased glycolytic flow characterizes glioblastoma cells. A metabolic reprogramming with agents able to inhibit carbohydrate metabolism might be a strategy to complement other therapeutics in the treatment of these tumours. We found that in GL15 glioblastoma cells 3BP reduces dramatically ATP levels by inhibiting ATP synthesis in both cytosolic and mitochondrial compartments (Davidescu et al., 2015), although it may affect other cellular pathways (Chiasserini et al., 2017). Interestingly, in experiments *in vitro* using mitochondria isolated from rat brain 3BP was inhibitory towards malate/pyruvate and succinate dependent respiration from complexes I and II, respectively, although the respiration from glycerol-3-phosphate and ascorbate was preserved, indicating that this drug may have limited harmful effects on normal cells (Macchioni et al., 2014).

Therefore, if on one side 3BP is useful in helping to overcome drug resistance, on the other side the conditions to increase its effectiveness at the lowest concentration should be found, in order to minimize the toxic effect on normal cells. In this study, we used 3BP as a metabolic modifier in U118 glioblastoma cells and found that the biochemical mechanisms leading to cell vitality decline rely on mitochondrial ROS-dependent pathways. Indeed, the association of 3BP with antimycin A or menadione concentrations exhibiting mild toxicity highly sensitizes cells to the effect of the drug by increasing mitochondrial ROS, resulting in the potentiation of 3BP efficacy at lower concentrations, consistent with the goal to minimize the toxic effect towards non-cancer cells.

## 2. Materials and methods

### 2.1. Chemicals

3-Bromopyruvate (3BP), ATP Bioluminescent Assay Kit, 3-(4,5-dimethyl-2-thiazolyl)-2,5-diphenyl-2H-tetrazolium bromide (MTT), 2',7'-dichlorodihydrofluorescein diacetate (H<sub>2</sub>DCFDA), MitoTEMPO, antimycin A, menadione, perifosine, digitonin, staurosporine, erythrosin B, LC3 rabbit polyclonal antibody, and actin mouse monoclonal antibody were from Sigma Aldrich. Cyt c mouse monoclonal, COX-IV mouse monoclonal, p53 mouse monoclonal, goat anti-mouse HRP-conjugated IgG, goat anti-rabbit HRP-conjugated IgG, and rabbit anti-goat HRP-conjugated IgG antibodies

were from Santa Cruz Biotechnology. Akt rabbit polyclonal, p-Akt (Ser-473) rabbit monoclonal, JNK rabbit monoclonal, p-JNK (Thr183/Tyr185) rabbit monoclonal, p44/42 MAPK (ERK1/2) rabbit monoclonal, p-ERK1/2 (Thr202/Tyr204) rabbit monoclonal, p38 MAPK rabbit polyclonal, p-p38 (Thr180/Tyr182) rabbit monoclonal, p-p53 (Ser-15) rabbit polyclonal, caspase-3 rabbit polyclonal, and caspase-9 rabbit polyclonal antibodies were from Cell Signaling Technology. Beta tubulin mouse monoclonal antibody was from Proteintech. 5,5',6,6'-tetrachloro-1,1',3,3'-tetraethylbenzimidazolylcarbocyanine iodide (JC-1) and MitoSOX™ were from Molecular Probes.

### 2.2. Cell culture and treatments

The following cell lines were obtained from the ATCC (Manassas, VA, USA): U-118 (HTB-15™) and U-87 (HTB-14™) human MG glioblastoma cells; rat-transformed EGCs (EGC/PK060399egfr; CRL-2690™); HEK-293 (CRL-1573™). The U-251 glioblastoma cell line was from CLS Cell Lines Service (300385). Glioblastoma cells were grown in Dulbecco's modified Eagle medium (DMEM, Himedia) supplemented with 10% fetal bovine serum (GIBCO), 100 µg/ml streptomycin, 100 U/ml penicillin, and 100 µg/ml gentamycin. U-118 cells were used throughout the work. In selected experiments, U-251 and U-87 cells, and non-tumoral EGC and HEK-293 cells were used for comparison with U-118. EGCs and HEK-293 were grown in Dulbecco's modified Eagle medium (GIBCO) supplemented with 10% heat inactivated fetal bovine serum (GIBCO), 100 µg/ml streptomycin and 100 U/ml penicillin.

Cells were mycoplasma-negative by qRT-PCR (forward primer: 5'-GGGAGCAAACAGGATTAGATACCCT-3'; reverse primer: 5'-TGCAC-CATCTGTCACTCTGTTAACCTC-3'). For treatments, cells were trypsinized and plated on 6-well plates (0.3 × 10<sup>6</sup>/well); for oxygen consumption and cyt c release experiments, cells were plated on T-75 flasks (2.5 × 10<sup>6</sup>). Cells were incubated for one day at 37 °C in a 5% CO<sub>2</sub> humidified atmosphere to obtain semi-confluent cells and the day before treatment medium was changed to serum-free DMEM. Buffered solutions of 3BP (pH 7.4) were used in the range of 10–100 µM for 2 h. Where indicated, cells were treated for 2 h with antimycin A (5–50 µM), valinomycin (1 µM), perifosine (2.5 or 5 µM), or staurosporine (1 µM, 2–24 h). In some experiments, antimycin A (5 µM), or menadione (15 µM), or perifosine (5 µM) were added 30 min before treatment with 3BP. Where indicated, cells were pre-treated for 1 h with 200 µM MitoTEMPO.

### 2.3. MTT and cell viability

MTT assay measures the metabolic reduction of MTT (yellow) to formazan (blue), due to the reducing power of electron flow along the respiratory chain, as well as to the activity of cytosolic dehydrogenases, thus representing a parameter of cellular vitality. Cells were grown and treated as described, then recovered, incubated with 0.5 mg/ml MTT for 1 h at 37 °C, and dissolved in 200 µl DMSO. Reduced MTT was evaluated by measuring the absorbance at 550 nm.

Cell viability was estimated using the erythrosin B exclusion assay by mixing 50 µL of cell suspension with 50 µL of 0.1% erythrosin in PBS. Counts were performed in triplicate under a 10× objective.

### 2.4. Cell permeability: PI and LDH assays

For propidium iodide (PI) assay, treated U118 cells (10<sup>6</sup>) were added with PI (10 µM) in isotonic PBS (2 ml) and fluorescence at 604 nm ( $\lambda_{ex}$  535 nm) was determined. For plasma membrane permeabilization with digitonin, 10<sup>6</sup> cells were incubated with 10 µg of digitonin for 10 min at 4 °C, recovered by centrifugation, and treated with PI as described above. The fluorescence elicited in the presence of 1% Triton X-100 was taken as 100%. Released and latent LDH activities were determined in the culture medium and in the cell pellet (10<sup>6</sup> cells) resuspended in the same volume of culture medium containing 1% Triton X-100. The reaction rate was

determined following NADH+H<sup>+</sup> oxidation at 340 nm in the presence of 1 mM pyruvate and 0.1 mM NADH + H<sup>+</sup>.

### 2.5. Annexin V-FITC/PI staining

To evaluate plasma membrane integrity and phosphatidylserine (PS) externalization as an early stage of apoptosis, flow cytometric analysis of annexin V-fluorescein isothiocyanate (FITC)/PI-stained U118 cells was performed using a commercial kit (Beckman Coulter) according to the manufacturer's instructions. Briefly, cells were resuspended in isotonic buffer (10<sup>6</sup> cells/ml) and co-stained with FITC-conjugated annexin V plus PI. After incubation at room temperature for 15 min, the stained cells were analysed by flow cytometry (EPICS-XL-MCL). As positive control, cells were incubated with 1 μM staurosporine for 18 h.

### 2.6. ATP determination

ATP levels were quantified by the ATP Bioluminescent Assay (FL-AA, Sigma) by using a calibrated ATP standard curve.

### 2.7. Fluorimetric determination of cellular ROS

For total intracellular ROS determination, treated U118 cells were stained for 30 min at 37 °C with 10 μM H<sub>2</sub>DCFDA and the elicited DCF fluorescence was measured (λ<sub>ex</sub> 485 nm, λ<sub>em</sub> 535 nm). For mitochondrial superoxide ion determination, cells were stained 30 min at 37 °C with 5 μM MitoSOX Red (λ<sub>ex</sub> 510 nm, λ<sub>em</sub> 600 nm). Fluorescence was determined using a Shimadzu RF-500 spectrofluorometer equipped with temperature control and magnetic stirrer device.

### 2.8. Glutathione peroxidase (GPx) activity

After treatment, 0.5 × 10<sup>6</sup> U118 cells were harvested and resuspended in 100 μl of GPx assay buffer (50 mM Na<sub>2</sub>HPO<sub>4</sub>, 0.1 mM EDTA, pH 7). Cells were sonicated and the resulting crude lysates were cleared by centrifuging at 14,000 rpm, for 10 min at 4 °C. GPx activity was determined using t-butyl hydroperoxide as substrate, following at 340 nm the rate of NADPH oxidation by the coupled reaction of glutathione reductase.

### 2.9. Catalase activity

Catalase activity was determined by measuring the decomposition of H<sub>2</sub>O<sub>2</sub> at 240 nm (molar extinction coefficient 39.4 M<sup>-1</sup> × cm<sup>-1</sup>). U118 cells (0.75 × 10<sup>6</sup>) were solubilized with 0.4% Triton X-100 and the activity was measured in phosphate buffer (pH 7.0). The specific activity was expressed as μmol H<sub>2</sub>O<sub>2</sub>/min/10<sup>6</sup> cells.

### 2.10. Mitochondrial membrane potential detection and oxygen consumption

Mitochondrial membrane potential (Δψ<sub>m</sub>) was determined by using the JC-1 fluorescent probe (1.5 μM), which changes colour from green to orange following Δψ<sub>m</sub> increase of mitochondria. JC-1 fluorescence was detected as described (Macchioni et al., 2018), and green/red fluorescence emission (FL1/FL2) of particles was reported as a dot plot. The uncoupler valinomycin (1 μM) was used to provide depletion of Δψ<sub>m</sub> (positive control). Flow cytometry analysis was performed using an EPICS XL-MCL (Beckman Coulter). Data were analysed by a data management system (Expo 32 software, Beckman Coulter, UK). Oxygen consumption in intact cells was determined with an oxytherm Clark-type electrode (Hansatech Instruments, Norfolk, UK). After incubation for 2 h with 20 μM 3BP or 10 μM CCCP, 5 × 10<sup>6</sup> cells were resuspended in 1 ml of respiration buffer (137 mM NaCl, 5 mM KCl, 0.7 mM NaH<sub>2</sub>PO<sub>4</sub>, 10 mM glucose, and 25 mM Tris-HCl, pH 7.4). Oxygen concentration was

recorded into a thermostatic chamber at 37 °C with stirring. The medium contained about 200 nmol oxygen/ml at 37 °C.

### 2.11. Cytochrome c release

After treatments, U118 cells (5 × 10<sup>6</sup>) were resuspended in PBS and permeabilized with digitonin solution (10 μg digitonin/10<sup>6</sup> cells). After incubation for 10 min at 4 °C, cells were centrifuged at 10,000 × g for 5 min. The supernatant was collected as the cytosolic fraction. The pellet, which contained the mitochondrial fraction, was resuspended in boiling SDS loading buffer. Supernatant and pellet fractions were analysed by Western blotting.

### 2.12. Apoptotic cell detection

Apoptotic cells were quantified by flow cytometry analysis of DNA after PI staining (50 μg/ml) in hypotonic solution. For each sample, 10,000 events were recorded and cells with a hypodiploid DNA content were quantified as apoptotic cells (Macchioni et al., 2018).

### 2.13. Western blot

Cell lysates were subjected to SDS-PAGE (40 μg protein/lane) and electroblotting on nitrocellulose membranes. Immunoblots were revealed by enhanced chemiluminescence reagent (Bio-Rad). Images were acquired using the VersaDoc 1000 imaging system and individual band densities were integrated by Quantity One software (BioRad) (Macchioni et al., 2017). In all the experiments shown, samples in horizontal lanes belong to the same gel, without cropping.

### 2.14. Statistical analyses

The results, expressed as means ± SD of at least three independent experiments, were analysed for statistical significance by Student's t-test; p-values < 0.05 were considered significant.

## 3. Results

### 3.1. 3BP effect on U118 cells vitality

We first assayed the experimental conditions to analyse the metabolic changes produced by the drug and found that the treatment with 10–80 μM 3BP produced effects on ATP levels and MTT already at 2 h incubation time, without any further variations up to 6 h (data not shown). Therefore, we selected 2-hour treatment throughout the work. Cells produce ATP through glycolysis and mitochondrial oxidative phosphorylation. In U118 cells, the mitochondrial inhibitor antimycin A (5–10 μM) reduced ATP levels by about 50%, compared to non-treated cells, which represents a control of mitochondrial contribution to ATP synthesis in these cells. 3BP reduced ATP levels starting from 20 μM concentration and caused almost complete ATP depletion at 40 μM, suggesting the inhibition of ATP synthesis in both mitochondrial and cytosolic compartments (Figure 1A). Alterations in cell morphology, including the loss of cell protrusions and the formation of round-shaped cells, were observed starting from 20 μM and interested most cells at 40 μM 3BP (Figure 1B), which also induced cell detachment from the culture plate. MTT reduction decreased significantly starting from 40 μM 3BP, indicating a decline of cellular activity (Figure 1C). The calculated IC<sub>50</sub> for 3BP was 41.4 μM (Figure 1C, insert). Plasma membrane integrity, evaluated by permeability to PI, LDH release, and erythrosine B stain of cells, was maintained up to 30 μM 3BP (Figures 1D–1F). Flow cytometry of FITC-annexin V/PI stained cells indicated that no PS exposure to the plasma membrane occurred up to 40 μM 3BP. The pool of PI permeable necrotic cells increased to about 37% at 40 μM 3BP (Figure 1G). Moreover, the LC3-II/LC3-I ratio did not increase, suggesting that cells were not addressed to autophagy (Figure 1H).

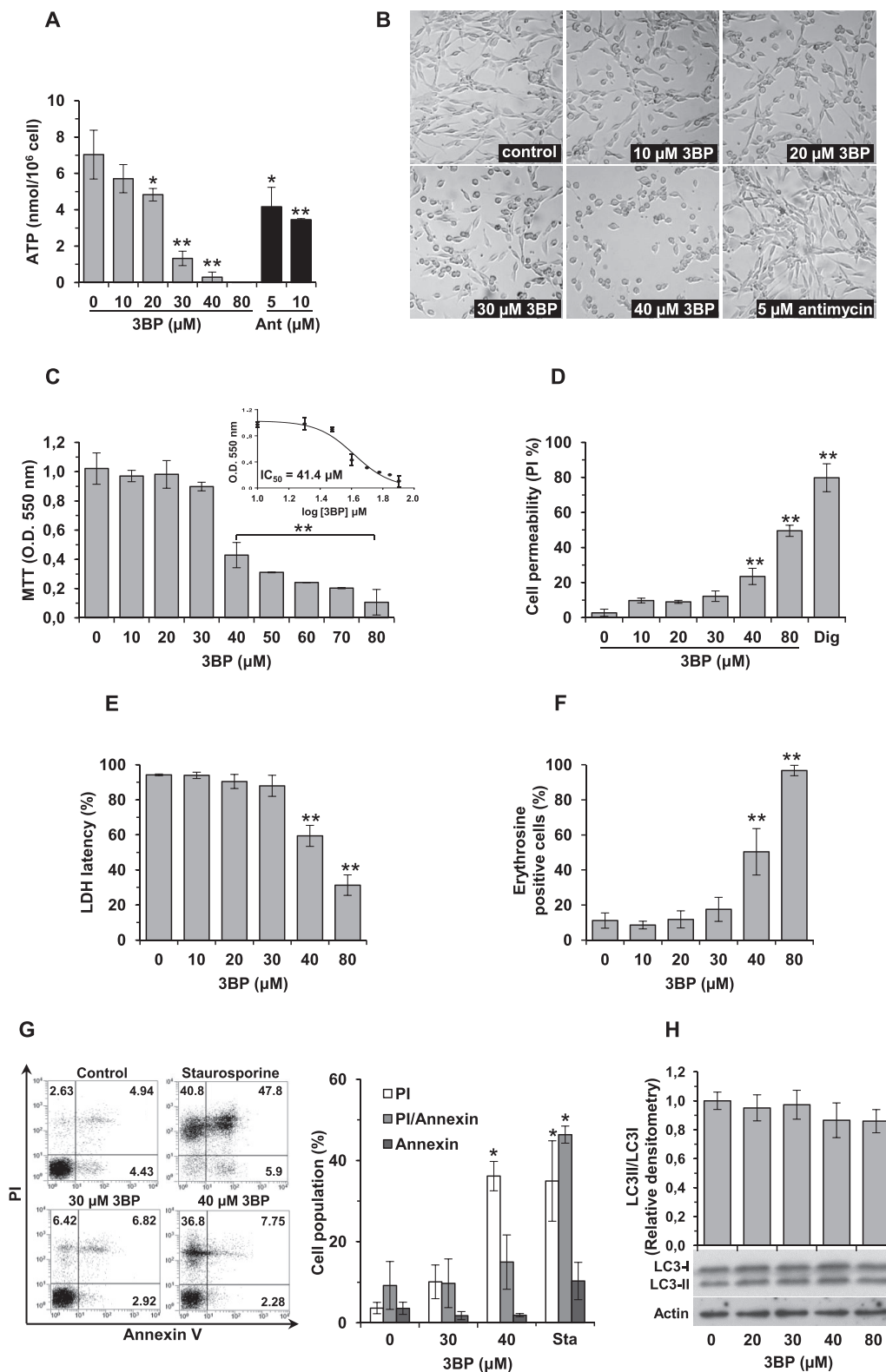


**Figure 1.** 3BP effect on U118 cells vitality parameters. Cells were subjected to 3BP or antimycin (Ant) treatments for 2 h and analysed. (A) ATP levels. (B) Cytopathic effect of 3BP. Images were acquired by an optical phase-contrast microscope equipped with a digital camera (20x magnification). Antimycin (5  $\mu\text{M}$ ) does not exert cytopathic effect. (C) MTT reduction assay. (D) Cell permeability to PI measured as fluorescence of 3BP-treated cells in isotonic solution. Digitonin (Dig) was a positive control for plasma membrane permeabilization. PI fluorescence in the presence of 1% Triton X-100 was taken as 100%. (E) LDH latency was determined as percent of LDH activity retained in the cell pellet. (F) Erythrosine positive cells. (G) For the evaluation of PS externalization, treated cells were stained with annexin V-FITC/PI and analysed by flow cytometry. Staurosporine (Sta, 1  $\mu\text{M}$ , 18 h) was used as positive control. Dot plot distribution of particles reporting annexin V-FITC fluorescence versus PI fluorescence is shown. Histograms show the percent of cell population exhibiting PI, PI/annexin, and annexin fluorescence. (H) Western blot analysis of the autophagy marker LC3. Data are the mean  $\pm$  SD of three independent experiments (\* $p < 0.05$ , \*\* $p < 0.01$ ). The full blot images are available as Supplementary material-original blottings.

### 3.2. 3BP triggers ROS production in U118 cells

Fluorimetric measurement of total intracellular ROS was performed in cells labelled with H<sub>2</sub>DCFDA. ROS levels increased at 30 and 40  $\mu$ M 3BP, compared to untreated cells, and their production at 30  $\mu$ M 3BP was significantly enhanced in the presence of the complex III inhibitor antimycin A at 5  $\mu$ M concentration (Figure 2A). The effect of antimycin at 40  $\mu$ M 3BP was less evident, probably due to cell damage observed at this 3BP concentration. The potentiating effect of antimycin in 3BP-triggered ROS production suggests the involvement of mitochondria. Indeed, the fluorescence of MitoSOX, a probe specifically sensitive to O<sub>2</sub> produced in the mitochondrial compartment, increased at 30 and 40  $\mu$ M 3BP (Figure 2B), demonstrating that mitochondria contribute to ROS production in 3BP-treated cells. Moreover, 5  $\mu$ M antimycin increased the MitoSOX fluorescence in the absence of 3BP, but also potentiated 3BP effect (Figure 2B). Since cell ROS levels come from the balance between their production and their disposal, we analysed glutathione peroxidase (GPx) and catalase activities in 3BP-treated cells, considering that 3BP is a -SH/-SeH blocker in proteins. Indeed, GPx activity was decreased in 3BP-treated cells, whereas catalase was not affected (Figure 2C). Therefore, the potential activity of GPx in maintaining antioxidative protection is lost following the treatment with 3BP due the presence of -SH groups in the protein.

### 3.3. 3BP treatment and mitochondrial bioenergetics of U118 cells

Mitochondrial ROS production prompted us to investigate whether 3BP affects mitochondrial energetics. First, we evaluated mitochondrial membrane potential ( $\Delta\psi_m$ ) by flow cytometry analysis of cells labelled with JC-1. Treatment with up to 40  $\mu$ M 3BP for 2 h did not impair  $\Delta\psi_m$ . Contrarily, the increased percentage of the cell population at high fluorescence indicated a small, but significant increase of  $\Delta\psi_m$ , pointing out membrane hyperpolarization (Figure 3A). Interestingly, the ATP decrease observed at 20–40  $\mu$ M 3BP (Figure 1A) and the concomitant  $\Delta\psi_m$  increase suggest that the

hyperpolarization status of the inner mitochondrial membrane is consequent to uncoupling. Indeed, the slope of oxygen consumption kinetics increased with 3BP (Figure 3B).  $\Delta\psi_m$  collapsed at 80  $\mu$ M 3BP, with cells localized in the low potential sector (Figure 3A). Valinomycin, which allows penetration of K<sup>+</sup> through the mitochondrial membrane and the discharge of the membrane potential, and the complex III inhibitor antimycin at 50  $\mu$ M concentration were positive controls for  $\Delta\psi_m$  depletion. However, 5  $\mu$ M antimycin did not alter cell population distribution (Figure 3A).

### 3.4. 3BP affects Akt and p53 in U118 cells

3BP was effective in deactivating two important factors for the survival and growth of tumour cells, Akt and p53. At 3BP concentrations higher than 20  $\mu$ M, Akt, which is constitutively phosphorylated and activated in U118 cells, was gradually dephosphorylated, without any effect on total Akt levels. At the same concentrations, 3BP favoured the gradual disappearance of both phosphorylated (Ser-15) and total p53 protein (Figure 4).

### 3.5. 3BP induces cytochrome c release without triggering an apoptotic cascade in U118 cells

Since mitochondrial ROS production generates H<sub>2</sub>O<sub>2</sub> that can diffuse to the cytosol, we analysed the MAPK pathway activation in response to ROS. Indeed, after 2-hour treatment with 3BP, JNK and ERK<sub>1/2</sub> phosphorylation increased, without any apparent changes in total protein expression, whereas p38 phosphorylation was not affected (Figure 5).

ROS production in mitochondria and MAPKs activation in the cytosol are the requisite that favour cytochrome c (cyt c) detachment from the inner mitochondrial membrane into a soluble cyt c pool in the intermembrane space, and the opening of mPTP to release cyt c outside mitochondria, respectively. During the treatment of U118 cells with 40  $\mu$ M 3BP for 2 h, about 28% of total cyt c left its natural localization in

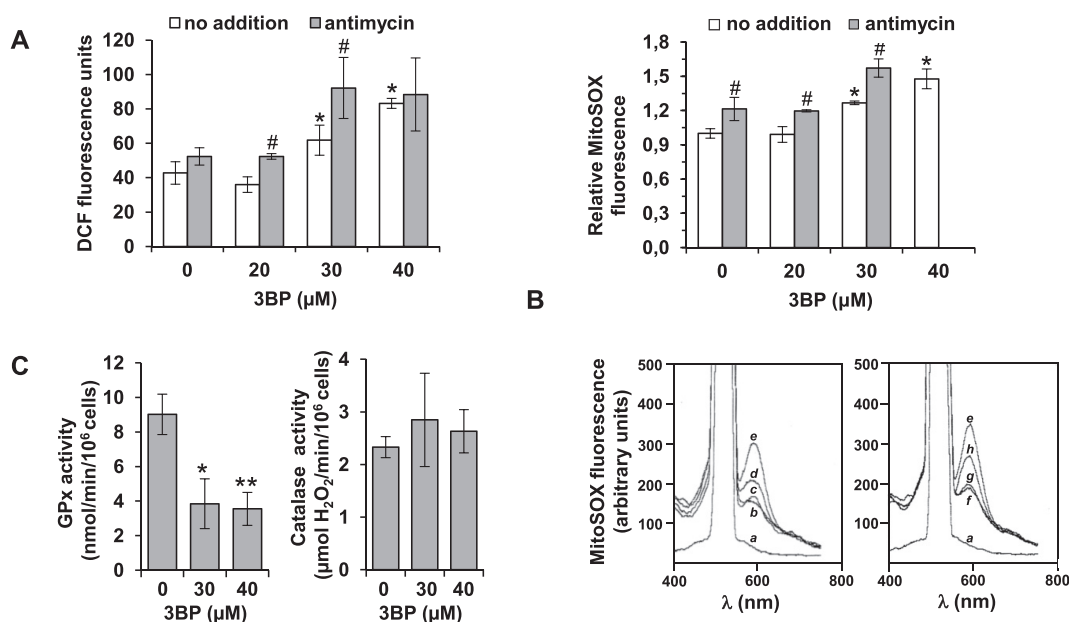


**Figure 2.** 3BP-induced ROS production in U118 cells. Cells were treated with 3BP for 2 h in the absence or presence of 5  $\mu$ M antimycin A. (A) For total intracellular ROS detection cells were stained with 10  $\mu$ M H<sub>2</sub>DCFDA and DCF fluorescence was reported as detected fluorescence units. (B) Mitochondrial ROS were detected by staining cells with 5  $\mu$ M MitoSOX Red. Reported fluorescence values are relative to control untreated cells. Data are the mean  $\pm$  SD of three independent experiments (\* $p$  < 0.05 vs control, # $p$  < 0.05 vs 3BP treatment). The lower panel in B shows MitoSOX Red fluorescence spectra: (a) probe; (b) untreated cells; (c) 20  $\mu$ M 3BP; (d) 30  $\mu$ M 3BP; (e) 30  $\mu$ M antimycin A, positive control; (f) 5  $\mu$ M antimycin A; (g) 5  $\mu$ M antimycin A+20  $\mu$ M 3BP; (h) 5  $\mu$ M antimycin A+30  $\mu$ M 3BP. (C) Glutathione peroxidase and catalase activities in 3BP-treated cells. Data are the mean  $\pm$  SD of three independent experiments (\* $p$  < 0.05, \*\* $p$  < 0.01).

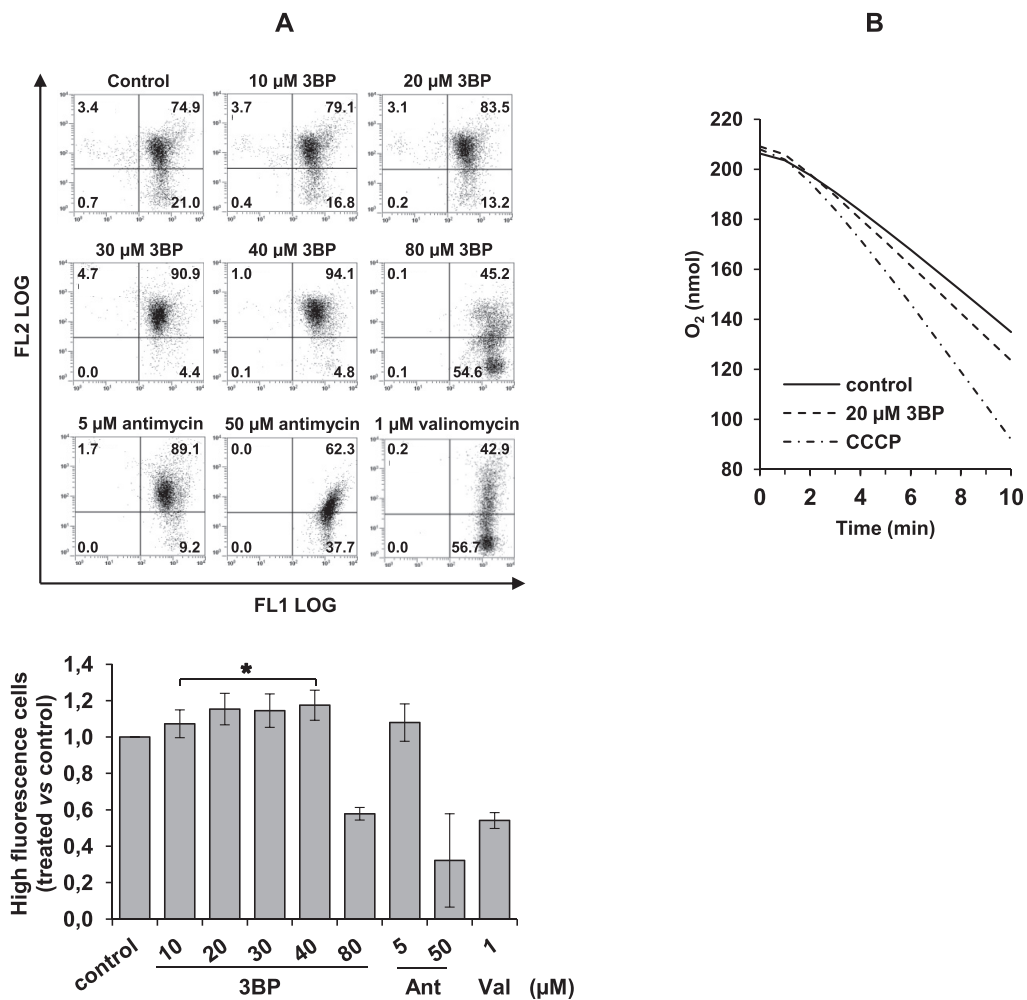


**Figure 3.** Mitochondrial membrane potential and oxygen consumption of 3BP-treated U118 cells. (A) Cells were incubated for 2 h in the presence of 3BP or antimycin (Ant). Thirty min before the end of incubation cells were loaded with JC-1 probe (1.5 μM), then recovered, resuspended in PBS, and analysed by flow cytometry. Valinomycin (Val) was a positive control for Δψm depletion. Each dot represents a single cell analysed for its green (FL1) and orange (FL2) associated fluorescence. Numbers in each quarter indicate the cell population percent. In the histogram, data are the mean ± SD of four independent experiments (\*p < 0.05). (B) Cells were incubated for 2 h with 3BP or CCCP, then resuspended in 1 ml of respiration buffer. Oxygen concentration was recorded as described in Materials and methods. The medium contained about 200 nmol oxygen/ml at 37 °C. A representative experiment of three is shown.

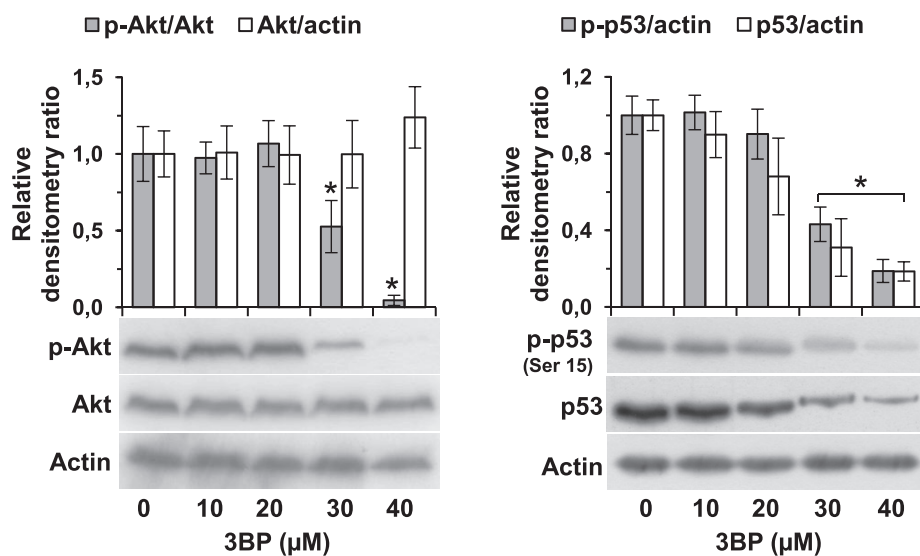


**Figure 4.** 3BP deactivates Akt and induces p53 degradation in U118 cells. Cells were subjected to 3BP treatments for 2 h and analysed by Western blotting for phosphorylated and total Akt or p53 proteins. Actin is a loading control. Each membrane was probed sequentially with phosphorylated and total protein antibodies, followed by actin antibody. Representative blots are shown. Data are the mean ± SD of three independent experiments (\*p < 0.05; \*\*p < 0.01). The full blot images are available as Supplementary material-original blottings.

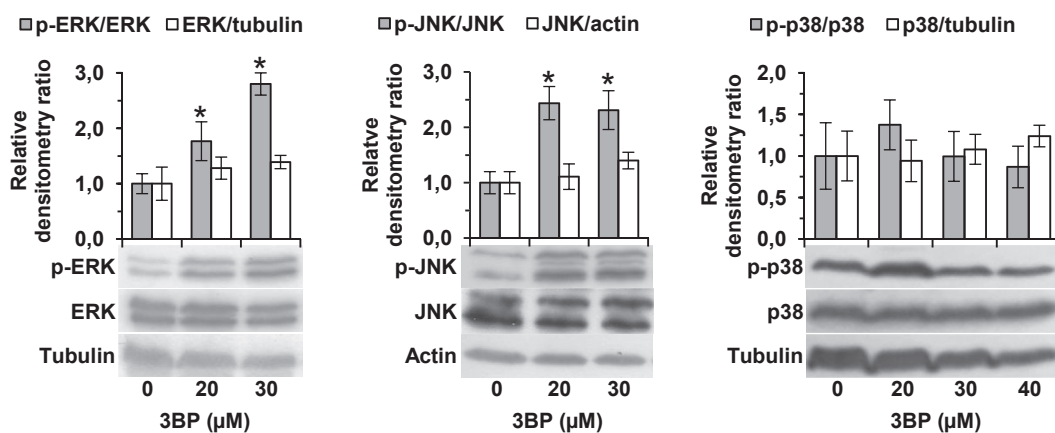


**Figure 5.** 3BP effect on MAPKs in U118 cells. Cells were subjected to 3BP treatments for 2 h and analysed by Western blotting for phosphorylated and total ERK, JNK, and p38 proteins. Actin and  $\beta$ -tubulin are loading controls. Each membrane was probed sequentially with phosphorylated and total protein antibodies, followed by actin or  $\beta$ -tubulin antibody. Representative images are shown. Data are the mean  $\pm$  SD of three independent experiments (\* $p < 0.05$ ). The full blot images are available as Supplementary material-original blottings.

mitochondria to translocate in the cytosolic compartment (Figure 6A). However, neither DNA fragmentation was observed at any tested 3BP concentration up to 24-hour treatment (Figure 6B), nor caspase-3 activation occurred after 2 h, as evidenced by the lack of the 19-kDa and 17-kDa fragments (Figure 6C). Upstream caspase-3, no caspase-9 activation

occurred in the presence of 3BP, rather 3BP was able to inhibit both caspase-3 and caspase-9 activation induced by staurosporine (Figures 6C and 6D). Therefore, although cyt c was present in the cytosol, 3BP hindered the cleavage of procaspase-9 to caspase-9 and the subsequent caspase-3 activation.

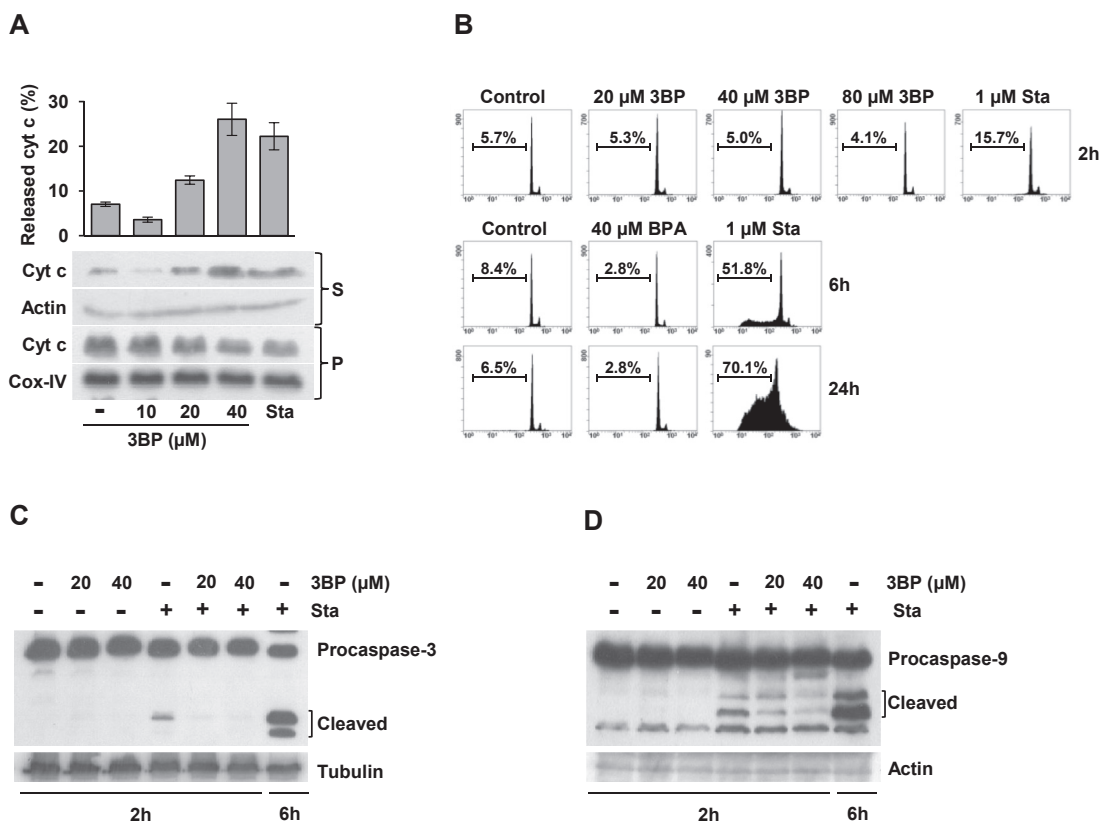


**Figure 6.** Cyt c released in 3BP-treated U118 cells does not trigger an apoptotic cascade. (A) Cells were incubated with 3BP for 2 h, harvested, permeabilized with digitonin, and centrifuged as described in Materials and methods. Western blotting was performed in the pellet (P) and in the supernatant (S). On volume basis, pellet samples loaded are one fourth of supernatants. Actin and COX-IV were analysed as loading controls. Distinct gels were performed for supernatant and pellet samples, and either gels or membranes were processed in parallel in the same conditions. After determination of blot densities, the amount of cyt c released in the supernatant was expressed as percentage  $\pm$ SD ( $n = 3$ ) of the total (pellet + supernatant), considering the loaded volumes. Staurosporine (Sta, 1  $\mu$ M) was a positive control. Representative blots of three are shown. (B) The percent of apoptotic cells (numbers in each plot) was evaluated by flow cytometry analysis of fragmented DNA after PI staining in hypotonic solution. (C and D) Western blot analysis of caspase-3 and caspase-9 cleaved fragments. Cells were incubated for the indicated times with 3BP and/or 1  $\mu$ M Sta (positive control for caspase activation) as indicated. Blots are representative of three independent experiments. The full blot images are available as Supplementary material-original blottings.

### 3.6. The ROS enhancers antimycin and menadione sensitize U118 cells to 3BP

The complex III inhibitor antimycin A hinders the electron flux from both complex I and complex II, whereas menadione, a substrate of flavoenzymes, produces semiquinone radicals. Incubation of U118 cells with 5  $\mu\text{M}$  antimycin or 15  $\mu\text{M}$  menadione for 2 h did not appreciably reduce cell vitality, as documented by MTT assay and erythrosine positive cells (Figure 7A). The rate of oxygen utilization was drastically reduced in the presence of antimycin, and by about 32% in the presence of menadione (Figure 7B). In parallel experiments, the extent of toxicity exerted by antimycin and menadione was evaluated in non-tumoral EGC and HEK-293 cells, finding that neither MTT nor the percent of erythrosine positive cells were affected (Figure 7A). However, antimycin produced a strong decrease on the rate of oxygen consumption, whereas menadione did not affect mitochondrial respiration (Figure 7B).

The finding that 5  $\mu\text{M}$  antimycin in association with 3BP increases ROS production (Figure 2) prompted us to investigate whether antimycin can potentiate the effect of 3BP on cell vitality. Indeed, starting from 30  $\mu\text{M}$  3BP, a concentration itself producing modest effects, the addition of 5  $\mu\text{M}$  antimycin significantly reduced the percent of MTT and live cells (Figures 8A and 8B). Interestingly, 5  $\mu\text{M}$  antimycin did not cause cyt c release outside mitochondria but, when in association with 3BP, it increased the 3BP-triggered cyt c release (Figure 8C), suggesting a prominent role of ROS in the potentiation of 3BP effect by antimycin. Yet, no caspase-3 activation occurred (Figure 8D).

To further investigate this issue, we used menadione, which generates ROS through redox cycling. Menadione itself was a modest ROS producer at 15  $\mu\text{M}$  concentration, but in combination with 30  $\mu\text{M}$  3BP it potentiated 3BP-induced ROS production (Figure 9A), together with MTT and

cell viability reduction (Figures 9B and 9C). In parallel, yet at 15  $\mu\text{M}$  concentration, menadione triggered cyt c release in the cytosolic compartment and increased 3BP-dependent cyt c release (Figures 9D and 9E). As expected, caspase-3 activation by menadione was contrasted by 30  $\mu\text{M}$  3BP (Figure 9F). By measuring MTT reduction, the potentiation of 3BP effect by antimycin and menadione was also observed in U251 and, restricted to antimycin, in U87 glioblastoma cells, even though the response in terms of 3BP concentrations is not overlapping, since the efficacy of 3BP can depend on the levels of reactive molecules towards 3BP in the specific cells (Figure 10).

Additional experiments were performed in U118 cells with the alkylphospholipid perifosine, which targets cell membranes as a membrane component. Perifosine is used in clinic for the treatment of malignancy. The efficacy of perifosine in our experimental conditions was demonstrated by Akt dephosphorylation (Figure 11A). Individually, both 5  $\mu\text{M}$  perifosine and 30  $\mu\text{M}$  3BP increased ROS production, as detected by DCF fluorescence, but their combination resulted in an additive effect, without potentiation (Figure 11B). Concomitantly, no potentiating effect was observed for MTT and cellular viability (Figures 11C and 11D). Interestingly, perifosine did not increase MitoSOX fluorescence (Figure 11E), thus excluding the mitochondrial origin of DCF-detected total ROS. Nevertheless, perifosine promoted cyt c release outside mitochondria (Figure 11F) and caspase-3 activation, again contrasted by 3BP (Figure 11G).

Following the observation that 3BP triggers ROS production and that cyt c release outside mitochondria is potentiated by antimycin, the effect of a ROS scavenger was investigated. As expected, when cells were incubated with 30  $\mu\text{M}$  3BP the addition of 5  $\mu\text{M}$  antimycin increased the pool of cyt c released in the cytosol. MitoTEMPO, a specific scavenger of mitochondrial superoxide, reduced the extent of the cyt c pool released

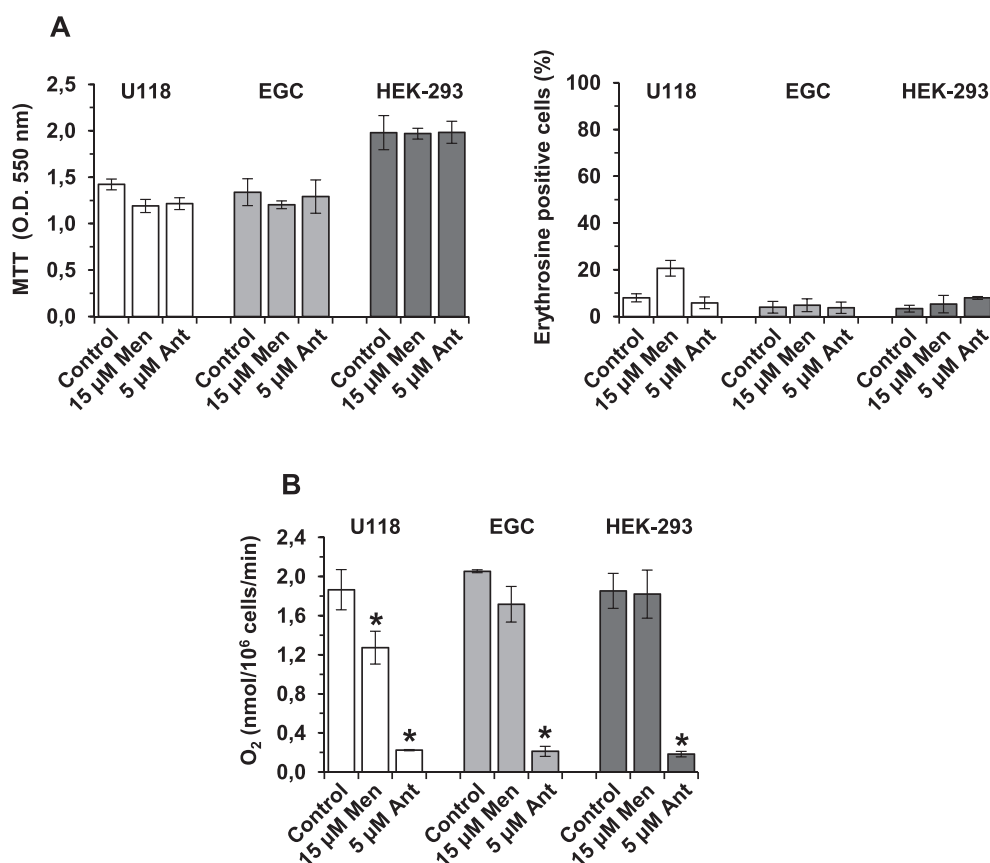


**Figure 7.** Effect of antimycin and menadione on vitality parameters of U118 and non-tumoral EGC and HEK-293 cells. Cells were incubated for 2 h with 5  $\mu\text{M}$  antimycin (Ant) or 15  $\mu\text{M}$  menadione (Men). (A) MTT reduction and erythrosine positive cells. (B) For the measurement of oxygen consumption, cells were resuspended in 1 ml of respiration buffer (see Materials and methods). Data are the mean  $\pm$  SD of three independent experiments (\* $p < 0.01$  vs control).

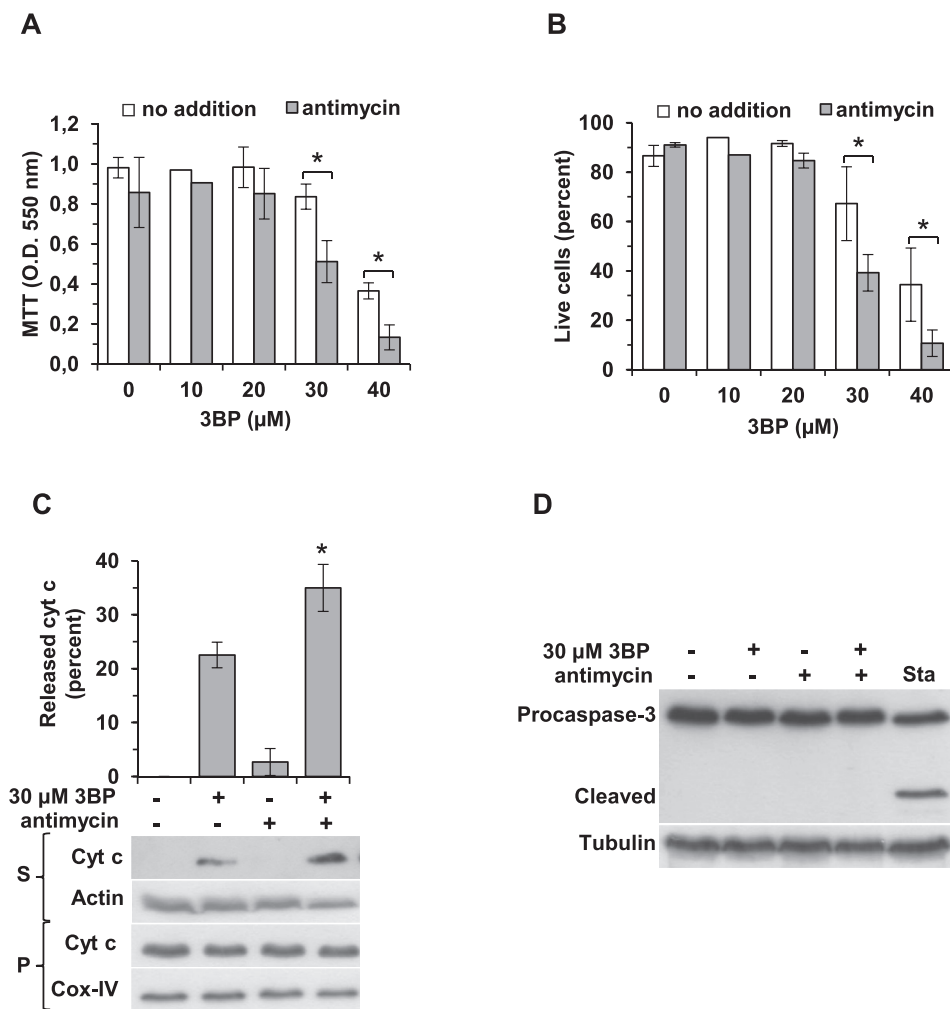


**Figure 8.** Antimycin A potentiates 3BP effects on cellular vitality and cyt c release in U118 cells. Cells were incubated with 3BP for 2 h without or with the addition of 5  $\mu\text{M}$  antimycin 30 min prior to 3BP. (A) MTT reduction assay. (B) Cell viability determined as the percent of erythroline negative cells. (C) Cyt c released in the supernatant was determined as described in the legend to Figure 6. Data are the mean  $\pm$  SD of three independent experiments (\* $p < 0.05$  vs 3BP). (D) Western blot analysis of caspase-3 cleaved fragments. Staurosporine (1  $\mu\text{M}$ , Sta) is a positive control for caspase-3 activation. The blot is representative of three independent experiments. The full blot images are available as Supplementary material-original blottings.

by 3BP or 3BP plus antimycin (Figure 12A), demonstrating that radicals are directly involved in the release of the protein outside mitochondria. At the same time, MitoTEMPO contrasted the effect of 3BP/antimycin association on both MTT and cellular viability decline (Figure 12B), reinforcing the identification of mitochondrial radicals as responsible for the diminished cellular vitality.

#### 4. Discussion

3BP is taken up via the monocarboxylate transporters (MCT-1) that are generally increased in activity in cancer cells (Baltazar et al., 2014; Pereira-Vieira et al., 2019), a condition that facilitates selective targeting of tumour cells, with healthy and non-malignant cells less influenced. In addition, the stability and the uptake of 3BP are favoured by the acidic environment of the tumour cells (Yadav et al., 2019). However, finding the lowest concentration of the drug producing metabolic reprogramming of tumour cells with the highest efficacy represents a primary research target. Here, we found that in U118 glioblastoma cells the vitality declined after treatment with 3BP by following a pathway dependent on the production of mitochondrial ROS. In addition, 3BP-induced ROS production increased in the presence of antimycin or menadione concentrations exhibiting mild toxicity, thus resulting in the potentiation of 3BP efficacy.

In U118 cells, plasma membrane leakage occurred at about 40  $\mu\text{M}$  3BP, but was not accompanied by PS exposure at plasma membrane level (Figure 1). Patterns of cell volume changes and plasma membrane phospholipid distribution during cell death are regarded as diagnostic of

distinguishing apoptosis from necrosis, the former being associated with cell shrinkage and early PS exposure, whereas necrosis is associated with cell swelling and consequent lysis. Therefore, 3BP directs U118 cells to a necrotic, non-apoptotic process. We previously demonstrated that in GL15, U251, and U87 glioblastoma cells 3BP causes ATP depletion and cell death, which follows different routes (Davidescu et al., 2015). In GL15 cells 3BP triggers pathways involving p53 dephosphorylation and its MDM2-dependent proteolysis, followed by irreversible autophagy that hinders the evolution towards apoptosis. Conversely, no autophagic response was elicited by 3BP in U87 and U251 (Davidescu et al., 2015), as well as in U118 glioblastoma cells.

Mitochondria as the target of 3BP action have been investigated in different experimental models, with effective doses ranging from 5 to 100  $\mu\text{M}$  (Galina, 2014; Rodrigues-Ferreira et al., 2012; Pereira da Silva et al., 2009). Following 3BP treatment of U118 cells, the quote of ATP produced in mitochondria was drastically reduced (Figure 1), whereas oxygen consumption increased as a consequence of uncoupling. This response is in agreement with the gradual increase of  $\Delta\psi\text{m}$  up to 40  $\mu\text{M}$  3BP (Figure 3) and with previous data relating an increase in  $\text{O}_2$  consumption to 3BP-induced mPTP, which is in accordance to the uncoupled increased rates of respiration (Rodrigues-Ferreira et al., 2012).

Glioblastoma cells are particularly refractory to apoptosis since they present constitutively activated Akt (pAkt) and mutated p53. These factors, essential to sustain U118 vitality, are targeted by 3BP that causes pAKT dephosphorylation and p53 degradation (Figure 4). Wild-type p53 exerts its role of tumour suppressor through several cysteine residues of the protein that are involved in site-specific DNA binding to control the

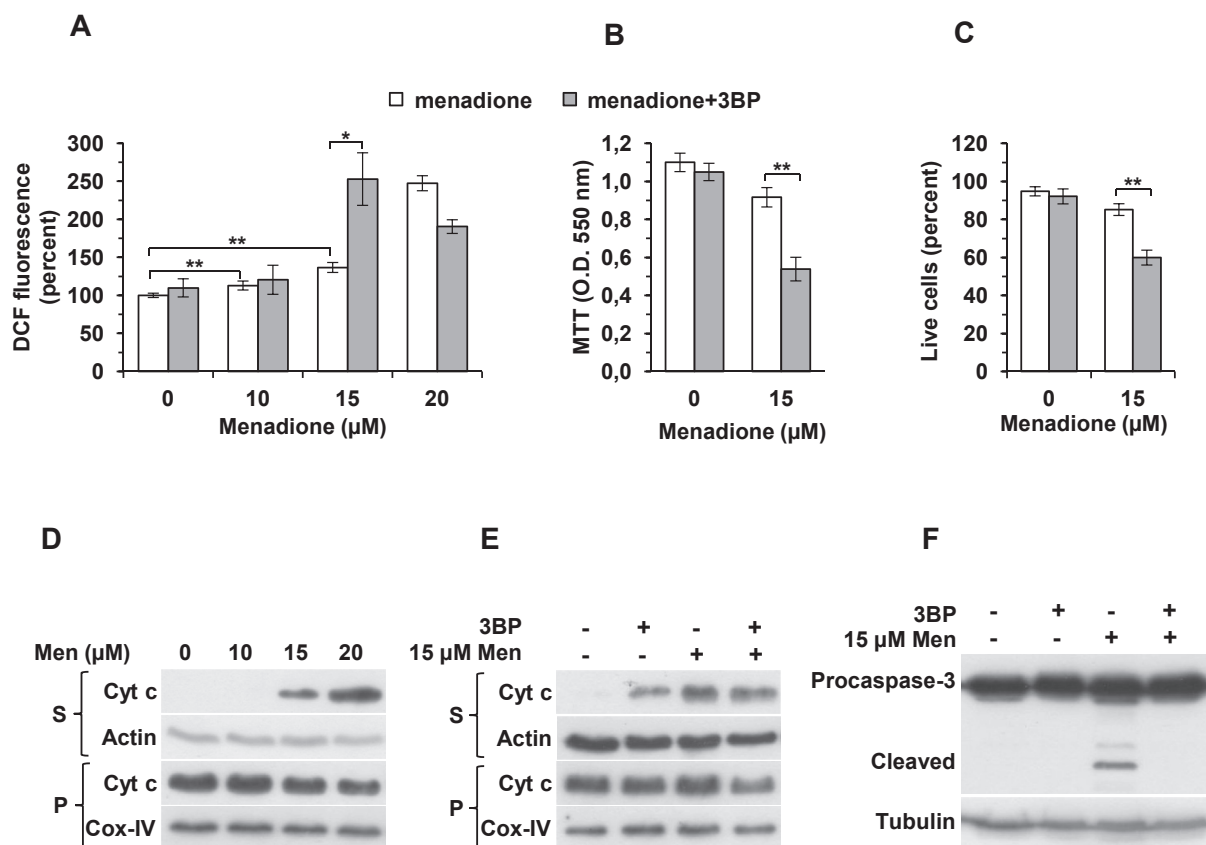


**Figure 9.** Menadione potentiates the effect of 3BP in U118 cells. Cells were incubated with 30 μM 3BP for 2 h without or with the addition of the indicated menadione (Men) concentrations 30 min prior to 3BP. (A) Total intracellular ROS were detected by staining cells with 10 μM H<sub>2</sub>DCFDA. (B) MTT reduction assay. (C) Cell viability determined as the percent of erythrosine negative cells. Data are the mean ± SD of three independent experiments (\*p < 0.05, \*\*p < 0.01). (D and E) Cyt c released in the supernatant was determined as described in the legend to Figure 6. (F) Western blot analysis of caspase-3 cleaved fragments. Tubulin was a loading control. Representative blots of three are shown. The full blot images are available as Supplementary material-original blottings.

expression of cell cycle and apoptosis genes (Rainwater et al., 1995). The p53 is a regulatory redox-sensitive protein that is addressed to degradation by thiol-conjugating drugs such as disulfiram, which acts on both wild-type and mutant p53 (Paranjpe and Srivenugopal, 2013). Therefore, we can argue that in U118 cells p53 is alkylated by 3BP at the level of cysteine residues, a modification that targets the protein to proteolysis. Hence, 3BP exerts a dual action, as alkylating and reactive reagent for -SH groups, and as ROS generator in mitochondria (Figure 2). ROS could be responsible for cardiolipin peroxidation due to the peroxidase activity acquired by cyt c, resulting in the weakening of cyt c-cardiolipin

interactions and cyt c detachment (Macchioni et al., 2011b). Spreading of ROS from mitochondria to the cytosol activates ERK and JNK (Figure 5), which are components of the serine/threonine MAPKs family involved in signal transduction from cell membranes to the nucleus (Macchioni et al., 2017; Brown and Sacks, 2009). The p38, a subgroup of MAPKs family, is usually activated by several stimuli (Matsuzawa and Ichijo, 2008). However, in U118 cells p38 is already constitutively activated, no apparent effects being exerted by 3BP (Figure 5). Therefore, after 3BP treatment U118 cells should be settled for channelling to apoptotic fate (Morrison, 2012). Indeed, components of the Bcl-2 family of proteins,

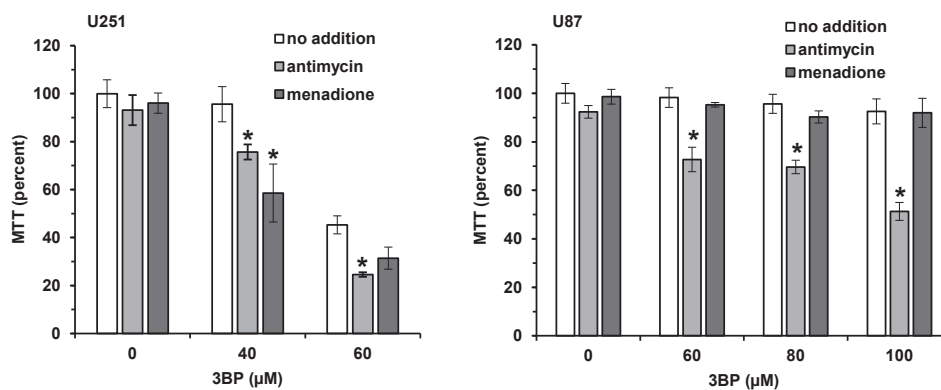


**Figure 10.** Effect of antimycin and menadione on the potentiation of 3BP effect in U251 and U87 glioblastoma cells. Cells were incubated with 3BP for 2 h without or with the addition of 5 μM antimycin or 15 μM menadione 30 min prior to 3BP, and MTT reduction was determined. Data are the mean ± SD of three independent experiments (\*p < 0.05 vs 3BP alone).

critical death regulators residing upstream of mitochondria (Scorrano and Korsmeyer, 2003), are phosphorylated by p-JNK, thus favouring the release of cyt c outside mitochondria (Figure 6). To note that in GL15, U87, and U251 glioblastoma cells 3BP causes cyt c degradation (Davidescu et al., 2015).

Usually, in the cytosol cyt c promotes the downstream apoptotic cascade by participating to the assembly of the cytosolic apoptosome (Riedl et al., 2005). In this pathway, the induction of apoptosis by different stimuli is associated with activation of aspartate-specific cysteine proteases (Martin and Green, 1995). Indeed, the recruitment

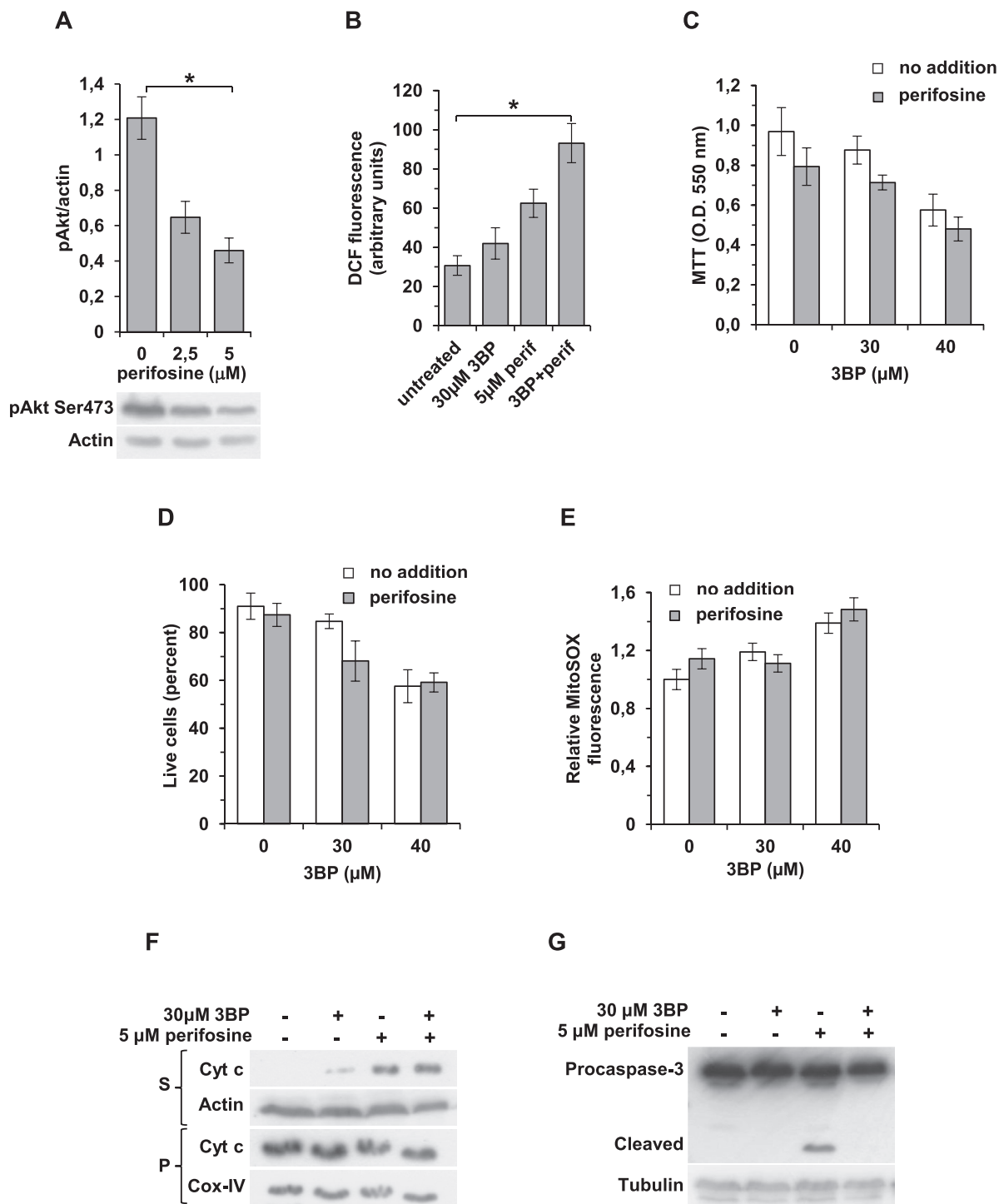


**Figure 11.** Perifosine does not potentiate 3BP effect in U118 cells. (A) Cells were incubated with 2.5 or 5 μM perifosine for 2 h and Akt Ser473 phosphorylation was analysed by Western blot. Actin was a loading control. (B–E) Cells were incubated with 3BP for 2 h without or with the addition of 5 μM perifosine 1 h prior to 3BP. (B) Total intracellular ROS were detected by staining cells with 10 μM H<sub>2</sub>DCFDA. (C) MTT reduction assay. (D) Cell vitality determined as the percent of erythrosine negative cells. (E) Mitochondrial ROS were detected by staining cells with 5 μM MitoSOX Red. Fluorescence was determined as described in Materials and methods. (F) Cyt c released in the supernatant was determined as described in the legend to Figure 6. (G) Western blot analysis of caspase-3 released fragments. Tubulin was a loading control. In A, F, and G, representative blots are shown. Data are the mean ± SD of three independent experiments (\*p < 0.05). The full blot images are available as Supplementary material-original blottings.

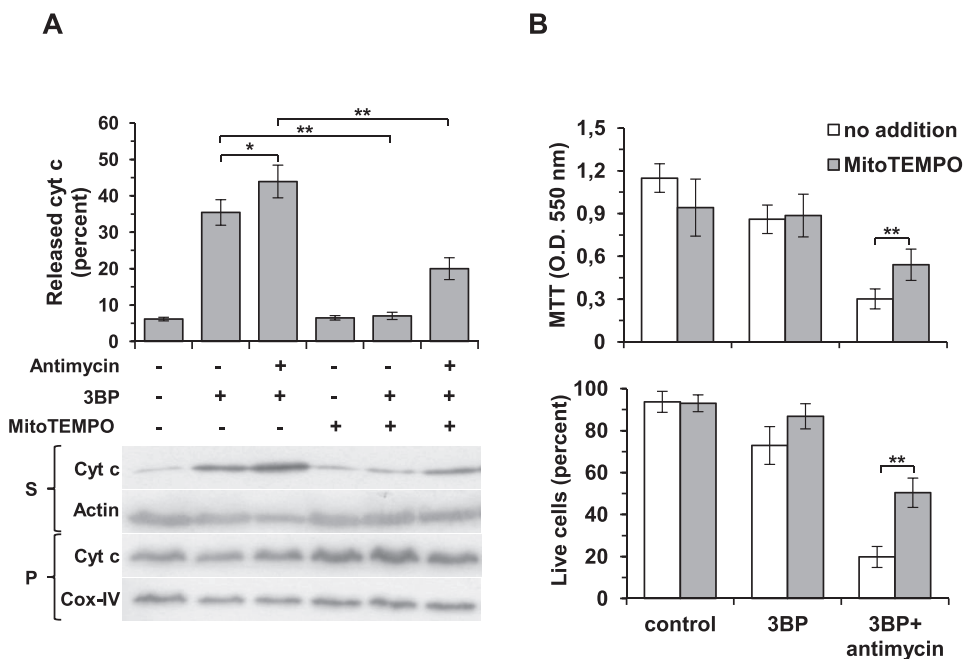


**Figure 12.** The ROS scavenger MitoTEMPO contrasts the potentiation of 3BP effect by antimycin in U118 cells. Cells were incubated with 30  $\mu$ M 3BP for 2 h in the presence of 5  $\mu$ M antimycin and/or 200  $\mu$ M MitoTEMPO. (A) Cyt c released in the supernatant was determined as described in the legend to Figure 6. On volume basis, pellet samples loaded are one half of supernatants. The blots are representative of three independent experiments. (B) MTT reduction assay and cell vitality determined as the percent of erythrosine negative cells. Data are the mean  $\pm$  SD of three independent experiments (\* $p < 0.05$ , \*\* $p < 0.01$ ). The full blot images are available as Supplementary material-original blottings.

of caspase-3 by caspase-9 occurs via interaction between the cysteine residue (C287) at the active site of caspase-9 and a critical aspartate (D175) in caspase-3 (Bratton et al., 2001), which leads to caspase-3 activation. Despite cyt c release in the cytosol following 3BP treatment of U118 cells, caspase-9 and caspase-3 activation and the consequent DNA fragmentation do not occur (Figure 6), which should be imputable to the reactivity of 3BP as an alkylating agent for -SH groups.

The efficacy of 3BP to kill U118 cells may be related also to its ability to imbalance the cellular redox state through the inhibition of GPx activity (Figure 2) or through interference with reduced glutathione (Galina, 2014). Indeed, the intracellular level of reduced glutathione can influence its efficacy, as demonstrated by the synergistic effect of GSH depletors (Niedźwiecka et al., 2016). Mitochondrial ROS cumulate in the presence of 3BP and further increase when 3BP is in combination with drugs that interfere with the electron flux in the respiratory chain. Antimycin stimulates ROS production from complex III and acts as an enhancer of 3BP-induced ROS (Figure 2). At the same time, 3BP efficacy in reducing MTT and cell viability is doubled in the presence of antimycin, and the amount of cyt c released in the cytosol increases (Figure 8). According to Thor et al. (1982), menadione can enter flavoprotein-catalyzed redox cycles with molecular oxygen and this can result in  $O_2^-$  production. In our experiments, menadione favours ROS accumulation and triggers concentration-dependent cyt c redistribution to the cytosol. Importantly, like antimycin, menadione potentiates the efficacy of 3BP on viability loss of U118 cells (Figure 9). Perifosine, which induces ROS of non-mitochondrial origin, does not potentiate the efficacy of 3BP (Figure 11), indicating the primary role of mitochondrial ROS in 3BP aggressiveness. Due to its chemical structure, perifosine acts as a detergent towards cell membranes (Vink et al., 2007). This justifies the detachment of cyt c from the inner mitochondrial membrane and its release in the cytosol to activate caspase-3, a process again inhibited by 3BP (Figure 11). Therefore, only mitochondrial ROS originating from the interference with the respiratory chain complexes are effective in potentiating 3BP activity. Indeed, when the ROS induced by 3BP were counteracted by MitoTEMPO, released cyt c decreased, and the potentiating effect of 3BP/antimycin association was weakened (Figure 12).

3BP, compared to other more specific antiglycolytics, acts as a metabolic modifier (Yadav et al., 2019) due to its specific chemical

reactivity, and produces loss of cell viability independently of the metabolic features of glioblastoma cells by inhibiting glycolysis and mitochondria-mediated bioenergetics. In U118 glioblastoma cells 3BP acts through a broad spectrum of inhibitory actions that produce metabolic changes leading to ATP depletion, an imbalance between production and disposal of mitochondrial ROS, and decline of cell survival.

This range of 3BP action may help overcome multidrug resistance consequent to drug primary action. It has been reported that valproate enhances 3BP-induced cell death of human glioblastoma cells through ATP depletion, due to MRP2 and BCRP valproate-dependent upregulation (Ishiguro et al., 2018). A recent emerging anticancer strategy consists in generating a redox imbalance in cells by promoting ROS overproduction or by inhibiting antioxidant systems activities. For example, ROS overproduction in cancer cells has been successfully obtained by combined treatment with menadione and ascorbate (Ren et al., 2019). In this study, we exploited the potential of 3BP as an anticancer drug able to trigger ROS production and, at the same time, to inhibit the GPx antioxidant system. By using in combination 3BP concentrations exhibiting low efficacy and antimycin or menadione, the efficacy of the drug against U118 glioblastoma cells was increased through a potentiating effect on 3BP-triggered ROS production. Interestingly, the potentiation of 3BP efficacy by antimycin and menadione can be extended to U251 and U87 glioblastoma cell lines. Menadione, contrarily to antimycin, did not affect respiration of non-tumour cells making it more suitable in combination with 3BP, in view of possible translational applications. Although 3BP cannot cross the blood-brain barrier, local delivery of the drug in high-grade gliomas in vivo was adopted successfully (Wicks et al., 2015). In addition, to overcome 3BP blood-brain barrier, new strategies aimed to find 3BP formulations that can facilitate drug delivering through the bloodstream are under investigation, with promising results (El Sayed, 2018). A recent review (Yadav et al., 2019) reports merits, demerits and limitations in the clinical application of this drug.

## 5. Conclusions

The metabolic modifier 3BP breaks down the viability of U118 glioblastoma cells by unbalancing mitochondrial ROS production and

disposal. The association of 3BP with antimycin or menadione highly sensitizes cells to the drug, lowering the effective 3BP concentrations, which can minimize the toxic effect towards non-cancer cells. Interestingly, the potentiation of 3BP efficacy by antimycin and menadione is common to other glioblastoma cell lines.

## Declarations

### Author contribution statement

Lanfranco Corazzi: Conceived and designed the experiments; Analyzed and interpreted the data; Contributed reagents, materials, analysis tools or data; Wrote the paper.

Lara Macchioni: Conceived and designed the experiments; Performed the experiments; Analyzed and interpreted the data; Wrote the paper.

Maya Petricciuolo, Magdalena Davidescu, Katia Fettucciari, Leonardo Gatticchi: Performed the experiments; Analyzed and interpreted the data.

Stefano Brancorsini: Analyzed and interpreted the data; Contributed reagents, materials, analysis tools or data.

Rita Roberti: Analyzed and interpreted the data; Wrote the paper.

### Funding statement

This research was supported by funds from Fondazione Cassa di Risparmio di Terni e Narni (grant J42F17000220007) and from Fondazione Cassa di Risparmio di Perugia, (grant 2017.0183.021 Ricerca Scientifica e Tecnologica).

### Data availability statement

Data included in article.

### Declaration of interests statement

The authors declare no conflict of interest.

### Additional information

Supplementary content related to this article has been published online at <https://doi.org/10.1016/j.heliyon.2020.e05741>.

## Acknowledgements

Carlo Alberto Ricci and Marcello Bianconi are thanked for skilful technical assistance.

## References

- Azevedo-Silva, J., Queirós, O., Baltazar, F., Ulaszewski, S., Goffeau, A., Ko, Y.H., Pedersen, P.L., Preto, A., Casal, M., 2016. The anticancer agent 3-bromopyruvate: a simple but powerful molecule taken from the lab to the bedside. *J. Bioenerg. Biomembr.* 48, 349–362.
- Baltazar, F., Pinheiro, C., Morais-Santos, F., Azevedo-Silva, J., Queirós, O., Preto, A., Casal, M., 2014. Monocarboxylate transporters as targets and mediators in cancer therapy response. *Histol. Histopathol.* 29, 1511–1524.
- Bechtel, W., Bauer, G., 2009. Catalase protects tumor cells from apoptosis induction by intercellular ROS signalling. *Anticancer Res.* 29, 4541–4558.
- Bratton, S.B., Walker, G., Srinivasula, S.M., Sun, X.-M., Butterworth, M., Alnemri, E.S., Cohen, G.M., 2001. Recruitment, activation and retention of caspases-9 and -3 by Apaf-1 apoptosome and associated XIAP complexes. *EMBO J.* 20, 998–1009.
- Brown, M.D., Sacks, D.B., 2009. Protein scaffolds in MAP kinase signalling. *Cell. Signal.* 21, 462–469.
- Burdon, R.H., 1995. Superoxide and hydrogen peroxide in relation to mammalian cell proliferation. *Free Radic. Biol. Med.* 18, 775–794.
- Chiasserini, D., Davidescu, M., Orvietani, P.L., Susta, F., Macchioni, L., Petricciuolo, M., Castigli, E., Roberti, R., Binaglia, L., Corazzi, L., 2017. 3-Bromopyruvate treatment induces alterations of metabolic and stress-related pathways in glioblastoma cells. *J. Proteomics* 152, 329–338.
- Choudhuri, S., Klaassen, C.D., 2006. Structure, function, expression, genomic organization, and single nucleotide polymorphisms of human ABCB1 (MDR1), ABCG2 (MRP), and ABCG2 (BCRP) efflux transporters. *Int. J. Toxicol.* 25, 231–259.
- Davidescu, M., Macchioni, L., Scaramozzino, G., Marchetti, M.C., Migliorati, G., Vitale, R., Corcelli, A., Roberti, R., Castigli, E., Corazzi, L., 2015. The energy blockers bromopyruvate and lonidamine lead GL15 glioblastoma cells to death by different p53-dependent routes. *Sci. Rep.* 5, 14343.
- El Sayed, S.M., 2018. Enhancing anticancer effects, decreasing risks and solving practical problems facing 3-bromopyruvate in clinical oncology: 10 years of research experience. *Int. J. Nanomed.* 13, 4699–4709.
- Fan, T., Sun, G., Sun, X., Zhao, L., Zhong, R., Peng, Y., 2019. Tumor energy metabolism and potential of 3-bromopyruvate as an inhibitor of aerobic glycolysis: implications in tumor treatment. *Cancers* 11, 317.
- Galina, A., 2014. Mitochondria: 3-bromopyruvate vs. mitochondria? A small molecule that attacks tumors by targeting their bioenergetic diversity. *Int. J. Biochem. Cell Biol.* 54, 266–271.
- Ganapathy-Kanniappan, S., Geschwind, J.-F.H., Kunjithapatham, R., Buijs, M., Syed, L.H., Rao, P.P., Ota, S., Kwak, B.K., Loffroy, R., Vali, M., 2010. 3-Bromopyruvate induces endoplasmic reticulum stress, overcomes autophagy and causes apoptosis in human HCC cell lines. *Anticancer Res.* 30, 923–936.
- Gottesman, M.M., 2002. Mechanisms of cancer drug resistance. *Annu. Rev. Med.* 53, 615–627.
- Ihrlund, L.S., Hermlund, E., Khan, O., Shoshan, M.C., 2008. 3-Bromopyruvate as inhibitor of tumour cell energy metabolism and chemopotentiator of platinum drugs. *Mol. Oncol.* 2, 94–101.
- Ishiguro, Y., Kobayashi, M., Ideno, M., Narumi, K., Furugen, A., Iseki, K., 2018. Valproate sensitizes human glioblastoma cells to 3-bromopyruvate-induced cytotoxicity. *Int. J. Pharm.* 551, 97–102.
- Kim, J.S., Ahn, K.J., Kim, J.-A., Kim, H.M., Lee, J.D., Lee, J.M., Kim, S.J., Park, J.H., 2008. Role of reactive oxygen species-mediated mitochondrial dysregulation in 3-bromopyruvate induced cell death in hepatoma cells. *J. Bioenerg. Biomembr.* 40, 607–618.
- Ko, Y.H., Niedźwiecka, K., Casal, M., Pedersen, P.L., Ulaszewski, S., 2019. 3-Bromopyruvate as a potent anticancer therapy in honor and memory of the late Professor André Goffeau. *Yeast* 36, 211–221.
- Lis, P., Dyląg, M., Niedźwiecka, K., Ko, Y.H., Pedersen, P.L., Goffeau, A., Ulaszewski, S., 2016. The HK2 dependent “Warburg Effect” and mitochondrial oxidative phosphorylation in cancer: targets for effective therapy with 3-bromopyruvate. *Molecules* 21, 1730.
- Macchioni, L., Davidescu, M., Sciacaluga, M., Marchetti, C., Migliorati, G., Coaccioli, S., Roberti, R., Corazzi, L., Castigli, E., 2011a. Mitochondrial dysfunction and effect of anticytolytic bromopyruvic acid in GL15 glioblastoma cells. *J. Bioenerg. Biomembr.* 43, 507–518.
- Macchioni, L., Davidescu, M., Mannucci, R., Francescangeli, E., Nicoletti, I., Roberti, R., Corazzi, L., 2011b. H<sub>2</sub>O<sub>2</sub> disposal in cardiolipin-enriched brain mitochondria is due to increased cytochrome c peroxidase activity. *Biochim. Biophys. Acta Mol. Cell Biol. Lipids* 1811, 203–208.
- Macchioni, L., Davidescu, M., Roberti, R., Corazzi, L., 2014. The energy blockers 3-bromopyruvate and lonidamine: effects on bioenergetics of brain mitochondria. *J. Bioenerg. Biomembr.* 46, 389–394.
- Macchioni, L., Davidescu, M., Fettucciari, K., Petricciuolo, M., Gatticchi, L., Gioè, D., Villanacci, V., Bellini, M., Marconi, P., Roberti, R., Bassotti, G., Corazzi, L., 2017. Enteric glial cells counteract *Clostridium difficile* Toxin B through a NADPH oxidase/ROS/JNK/caspase-3 axis, without involving mitochondrial pathways. *Sci. Rep.* 7, 45569.
- Macchioni, L., Petricciuolo, M., Davidescu, M., Fettucciari, K., Scarpelli, P., Vitale, R., Gatticchi, L., Orvietani, P.L., Marchegiani, A., Marconi, P., Bassotti, G., Corcelli, A., Corazzi, L., 2018. Palmitate lipotoxicity in enteric glial cells: lipid remodeling and mitochondrial ROS are responsible for cytochrome c release outside mitochondria. *Biochim. Biophys. Acta Mol. Cell Biol. Lipids* 1863, 895–908.
- Maiti, A.K., 2012. Reactive oxygen species reduction is a key underlying mechanism of drug resistance in cancer chemotherapy. *Chemotherapy* 1.
- Martin, S.J., Green, D.R., 1995. Protease activation during apoptosis: death by a thousand cuts? *Cell* 82, 349–352.
- Mathupala, S.P., Ko, Y.H., Pedersen, P.L., 2009. Hexokinase-2 bound to mitochondria: cancer’s stygian link to the “Warburg Effect” and a pivotal target for effective therapy. *Semin. Cancer Biol.* 19, 17–24.
- Matsuzawa, A., Ichijo, H., 2008. Redox control of cell fate by MAP kinase: physiological roles of ASK1-MAP kinase pathway in stress signalling. *Biochim. Biophys. Acta* 1780, 1325–1336.
- Morrison, D.K., 2012. MAP kinase pathways. *Cold. Spring. Harb. Perspect. Biol.* 4, a011254.
- Nakano, A., Tsuji, D., Miki, H., Cui, Q., El Sayed, S.M., Ikegame, A., Oda, A., Amou, H., Nakamura, S., Harada, T., Fujii, S., Kagawa, K., Takeuchi, K., Sakai, A., Ozaki, S., Okano, K., Nakamura, T., Itoh, K., Matsumoto, T., Abe, M., 2011. Glycolysis inhibition inactivates ABC transporters to restore drug sensitivity in malignant cells. *PLoS One* 6, e27222.
- Natarajan, K., Xie, Y., Baer, M.R., Ross, D.D., 2012. Role of breast cancer resistance protein (BCRP/ABCG2) in cancer drug resistance. *Biochem. Pharmacol.* 83, 1084–1103.
- Ni, L.-N., Li, J.-Y., Miao, K.-R., Qiao, C., Zhang, S.-J., Qiu, H.-R., Qian, S.-X., 2011. Multidrug resistance gene (MDR1) polymorphisms correlate with imatinib response in chronic myeloid leukemia. *Med. Onc.* 28, 265–269.
- Niedźwiecka, K., Dyląg, M., Augustyniak, D., Majkowska-Skrobek, G., Cal-Bąkowska, M., Ko, Y.K., Pedersen, P.L., Goffeau, A., Ulaszewski, S., 2016. Glutathione may have implications in the design of 3-bromopyruvate treatment protocols for both fungal and algal infections as well as multiple myeloma. *Oncotarget* 7, 65614–65626.
- Paranjpe, A., Srivenugopal, K.S., 2013. Degradation of NF-κB, p53 and other regulatory redox-sensitive proteins by thiol-conjugating and -nitrosylating drugs in human tumor cells. *Carcinogenesis* 34, 990–1000.

- Pereira da Silva, A.P., El-Bacha, T., Kyaw, N., Dos Santos, R.S., Da-Silva, W.S., Almeida, F.C.L., Da Polan, A.T., Galina, A., 2009. Inhibition of energy-producing pathways of HepG2 cells by 3-bromopyruvate. *Biochem. J.* 417, 717–726.
- Pereira-Vieira, J., Azevedo-Silva, J., Preto, A., Casal, M., Queirós, O., 2019. MCT1, MCT4 and CD147 expression and 3-bromopyruvate toxicity in colorectal cancer cells are modulated by the extracellular conditions. *Biol. Chem.* 400, 787–799.
- Rainwater, R., Parks, D., Anderson, M.E., Tegtmeyer, P., Mann, K., 1995. Role of cysteine residues in regulation of p53 function. *Mol. Cell Biol.* 15, 3892–3903.
- Ren, X., Santhosh, S.M., Coppo, L., Ogata, F.T., Lu, J., Holmgren, A., 2019. The combination of ascorbate and menadione causes cancer cell death by oxidative stress and replicative stress. *Free Radic. Biol. Med.* 134, 350–358.
- Riedl, J., Li, W., Chao, Y., Schwarzenbacher, R., Shi, Y., 2005. Structure of the apoptotic protease-activating factor 1 bound to ADP. *Nature* 434, 926–933.
- Rodrigues-Ferreira, C., Pereira da Silva, A.P., Galina, A., 2012. Effect of the antitumoral alkylating agent 3-bromopyruvate on mitochondrial respiration: role of mitochondrially bound hexokinase. *J. Bioenerg. Biomembr.* 44, 39–49.
- Scorrano, L., Korsmeyer, S.J., 2003. Mechanisms of cytochrome c release by proapoptotic BCL-2 family members. *Biochem. Biophys. Res. Commun.* 304, 437–444.
- Shoshan, M.C., 2012. 3-bromopyruvate: targets and outcomes. *J. Bioenerg. Biomembr.* 44, 7–15.
- Thor, H., Smith, M.T., Hartzell, P., Bellomo, G., Jewell, S.A., Orrenius, S., 1982. The metabolism of menadione (2-methyl-1,4-naphthoquinone) by isolated hepatocytes. A study of the implications of oxidative stress in intact cells. *J. Biol. Chem.* 257, 12419–12425.
- Vink, S.R., van Blitterswijk, W.J., Schellens, J.H.M., Verheij, M., 2007. Rationale and clinical application of alkylphospholipid analogues in combination with radiotherapy. *Cancer Treat. Rev.* 33, 191–202.
- Wicks, R.T., Azadi, J., Mangraviti, A., Zhang, I., Hwang, L., Joshi, A., Bow, H., Hutt-Cabezas, M., Martin, K.L., Rudek, M.A., Zhao, M., Brem, H., Tyler, B.M., 2015. Local delivery of cancer-cell glycolytic inhibitors in high-grade glioma. *Neuro Oncol.* 17, 70–80.
- Wintzell, M., Löfstedt, L., Johansson, J., Pedersen, A.B., Fuxe, J., Shoshan, M., 2012. Repeated cisplatin treatment can lead to a multiresistant tumor cell population with stem cell features and sensitivity to 3-bromopyruvate. *Cancer Biol. Ther.* 13, 1454–1462.
- Wu, L., Xu, J., Yuan, W., Wu, B., Wang, H., Liu, G., Wang, X., Du, J., Cai, S., 2014. The reversal effects of 3-bromopyruvate on multidrug resistance *in vitro* and *in vivo* derived from human breast MCF-7/ADR cells. *PLoS One* 9, e112132.
- Yadav, S., Pandey, S.K., Goel, Y., Temre, M.K., Singh, S.M., 2019. Diverse stakeholders of tumor metabolism: an appraisal of the emerging approach of multifaceted metabolic targeting by 3-bromopyruvate. *Front. Pharmacol.* 10, 728.